

Sub-30 nm thick plasmonic films and structures with ultralow loss

Cite this: DOI: 10.1039/c3nr05502g

Ee Jin Teo,^{*a} Noriaki Toyoda,^b Chengyuan Yang,^c Bing Wang,^a Nan Zhang,^a Andrew A. Bettiol^c and Jing Hua Teng^a

We report an alternative method of producing sub-30 nm thick silver films and structures with ultralow loss using gas cluster ion beam irradiation (GCIB). We have direct evidence showing that scattering from grain boundaries and voids rather than surface roughness are the main mechanisms for the increase in loss with reducing thickness. Using GCIB irradiation, we demonstrate the ability to reduce these scattering effects simultaneously through nanoscale surface smoothing, increase in grain width and lower percolation threshold. Significant improvement in electrical and optical properties by up to 4 times is obtained, before deviation from bulk silver properties starts to occur at 12 nm. We show that this is an enabling technology that can be applied post fabrication to metallic films or lithographically patterned nanostructures for enhanced plasmonic performance, especially in the ultrathin regime.

Received 16th October 2013
Accepted 10th December 2013

DOI: 10.1039/c3nr05502g

www.rsc.org/nanoscale

Introduction

Recently, there has been much research interest in sub-diffraction limit optical imaging and nanolithography using far-field hyperlens^{1–3} and near-field superlens.^{4,5} Omni-directional flat lensing with negative refractive index has also been demonstrated at ultraviolet wavelengths using multilayer Ag/TiO₂ plasmonic metamaterials.⁶ Long range surface plasmons waveguides made of 20 nm thick Au embedded in dye solution have been shown to have an optical gain of 8.55 dB mm⁻¹.⁷ Silver is often the material of choice due to its superior intrinsic properties such as low ohmic loss,⁸ high conductivity and reflectivity⁹ at visible wavelengths. However, the minimum sub-diffraction resolution limit and highest imaging contrast attainable is strongly dependent on the surface roughness and thickness of the metal film. For a pure Ag superlens, thickness is often limited to 20–30 nm, in order to reduce the loss in the Ag.¹⁰ Demand becomes more stringent in multilayer plasmonic metamaterials where thicknesses of 10 nm Ag are used.⁶ Surface roughness can significantly degrade the performance of these devices, since surface plasmons are strongly confined to the metal–dielectric interface. This has been shown previously by Liu *et al.*,¹¹ whereby a reduction in roughness from 5 to 2 nm in a superlens device can improve the contrast from 1.2 to 6.5.

Such requirements are difficult to achieve for Ag films formed by electron beam evaporation,¹² chemical vapor deposition,¹³ electroless plating¹⁴ and physical sputtering.¹⁵ Ag films deposition follows the Volmer–Weber growth model¹⁶ and has poor wettability on insulators due to the low surface energy. Therefore, films are polycrystalline and have a high surface root-mean-square (RMS) roughness. The formation of a continuous film of silver below the percolation threshold of ~10 nm does not occur. The percolation threshold is the point when a deposited metallic film transforms from being predominantly insulating to conducting. For films slightly above the percolation threshold, a large number of voids still exist between the islands and optical loss can be relatively high. Only at a thickness of more than 30 nm do the optical constants reach values that are similar to bulk silver.¹⁷ The inferior quality of these ultrathin films eventually places a fundamental limit on the achievable contrast and resolution of a superlens or hyperlens. It also shortens the propagation length of metallic waveguides and worsens the Q-factor of plasmonic resonators.

Previous attempts at overcoming this problem include using a seed layer such as Ge to reduce the surface roughness of a deposited silver film to less than 1 nm while still achieving a continuous film of 10 nm thick. Ge has a higher surface energy so Ag films that form on Ge are smoother and exhibit a lower percolation threshold. However, the loss in a Ge/Ag film does not improve and even gets worse, due to the extra damping loss caused by the seed layer and quantum size effect.^{18,19} As the nanocrystals formed in these ultrathin layers are small compared to the mean free path of electrons (~52 nm),²⁰ electrons experience a higher number of collisions with the grain boundaries, which can result in 5 to 10 times higher loss compared to bulk silver.^{20,21} Therefore for the same roughness, a

^aInstitute of Materials Research and Engineering, Agency for Science, Technology and Research (A*STAR), 3 Research Link, 117602, Singapore. E-mail: teoej@imre.a-star.edu.sg

^bJapan Graduate school of Engineering, University of Hyogo, 2167 Shosha, Himeji, Hyogo 671-2280, Japan

^cDepartment of Physics, National University of Singapore, 2 Science Drive 3, 117542, Singapore

Ag superlens with a Ge or Ni seed layer actually has 2 times poorer contrast compared to the one without the seed layer.^{11,22,23} Another surface roughness reduction approach²⁴ involves stripping the silver film from the substrate to reveal the ultra-smooth back surface. This approach, however, requires the use of epoxy for template release and does not improve the percolation threshold.

Previously, gas cluster ion beam (GCIB) technique has been used extensively to smooth magnetic materials for data storage, semiconductors for CMOS devices and diamond surfaces for industrial applications.^{25–28} GCIB treatment also enhances bio-integration and cells proliferation in bioimplants.²⁹ Although it is an established technique that is commercially available, it has not been used for plasmonics and metamaterials applications. In this work, we show that GCIB can effectively reduce scattering due to grain boundaries, voids and surface roughness so that enhanced surface plasmon resonance and propagation in silver films and waveguides is obtained. In this work, GCIB is carried out using a beam of N₂ gas cluster, consisting of thousands of molecules bounded by weak van der Waals forces. This is first produced by supersonic expansion of the high pressure gas as it passes through a shaped nozzle into vacuum. The cluster is then ionized by electron bombardment and accelerated to 20 keV before it is directed onto the sample. Upon impact, the cluster disintegrates into individual constituent atoms with an average energy of a few eV. Due to the high mass of each cluster and low energy/atom, a large energy density is delivered to a small volume with very low penetration depth. The target atoms are mostly ejected laterally from the impact site. This lateral distribution of sputtered atoms causes smoothing of irregularities on the surface, which is not achievable with monomer ion beams. The individual atoms of a few eV are not energetic enough to cause sub-surface damage, typically associated with plasma polishing, etching or ion milling process.

Experimental

In this study, a series of 70 nm thick Ag films are deposited onto glass microscope coverslips using conventional electron beam evaporation. The samples are cleaned ultrasonically in acetone for 5 min before Ag deposition using electron beam deposition (Denton Vacuum, Explorer) at a rate of 1 A s⁻¹. GCIB irradiation was then performed on the Ag films using 20 keV N₂ GCIB with doses from 1.0 × 10¹⁵ ions per cm² to 4.2 × 10¹⁶ ions per cm². Atomic force microscopy (AFM) and scanning electron microscopy (SEM) is used to characterize the film thickness, surface roughness and morphology of the films. We have studied the resistivity of as-deposited, Cr/Ag and GCIB processed films using the Hall effect (BioRad HL5500 system).

Surface plasmon resonance (SPR) spectroscopy has been used to determine the dielectric constant of Ag.^{30,31} This is carried out in Kretschmann configuration, consisting of a BK7 prism–silver–air system. A linearly polarized He–Ne laser light (5 mW, at 632.8 nm) is modulated by a chopper and passed through two polarizers for polarization control. The sample, BK7 prism, and photodiode detector are mounted onto the two

coaxial arms of a goniometer for precise angle scan of the incidence and reflection beam. Surface plasmons are excited by coupling laser light through the BK 7 prism. The reflected laser light is measured by a detector through a lock-in amplifier. All the depositions and characterizations were performed at room temperature. More details of the setup can be found in the literature.³²

Furthermore, GCIB has been applied to lithographically patterned Ag waveguides, whereby the propagation length is measured using WITec scanning near field optical microscopy (SNOM) system. Light from a 632.8 nm He–Ne laser is focused onto the grating coupler through the substrate. Surface plasmons propagating in the metal waveguide are collected in the near-field with a photomultiplier tube, *via* a Si tip with an aperture hole of 90 nm.

Results and discussion

Nanoscale control of film thickness, roughness and grain size

Fig. 1 shows the AFM images of the Ag surfaces measured over a 1 × 1 μm² area before and after irradiation with 1 × 10¹⁵, 5 × 10¹⁵ and 1 × 10¹⁶ ions per cm². For the as-deposited film, the surface exhibits a high level of faceting and surface roughness, caused by the polycrystalline growth. The maximum peak-to-valley height was measured to be $R_{\max} = 41.6$ nm, and the RMS roughness $\sigma = 4.9$ nm. By increasing the dose to 1 × 10¹⁶ ions per cm², we can see a smoothing of the surface, whereby R_{\max} is reduced to 13.1 nm and σ to 1.20 nm. At the same time, an increase in lateral grain size of up to 400 nm is observed with increasing dose.

We have plotted the change in σ and correlation length, L as a function of dose in Fig. 2a. According to (ref. 33), L corresponds closely to the grain size. Initially, we can see a sharp decrease in σ from 5 to 1.2 nm and increase in L from 44 to 152 nm with dose. After a dose of 7 × 10¹⁵ ions per cm², negligible change is observed as saturation is reached. Both effects are favorable for decreasing the scattering loss as electrons will experience fewer collisions with the grain boundaries and surface roughness. To date, there has not been a technique that can reduce these scattering effects simultaneously with nanometer precision. Deposition with a seed layer can improve the surface roughness but results in small grain sizes. Annealing can increase grain size but process is difficult to control and may worsen the surface roughness.

Besides smoothing the surface, the GCIB process can simultaneously thin down the metal layer. It can be seen from Fig. 2b that the film thickness linearly decreases from 70 nm down to 8.5 nm as the dose is increased from 1.0 × 10¹⁵ ions per cm² to 4.2 × 10¹⁶ ions per cm². By accurate control of dose, it is possible to obtain Ag layers that are ultrathin (<10 nm) and smooth (~1.2 nm) with large grain width.

Fig. 3a–c shows a schematic diagram of the effect of increasing dose on the polycrystalline Ag surface. A close-up view of the smoothing and thinning mechanism has been illustrated too. As the gas cluster bombards onto the surface at normal incidence, the lateral sputtering causes Ag atoms to be deposited on both sides of the hills. At oblique angles, the

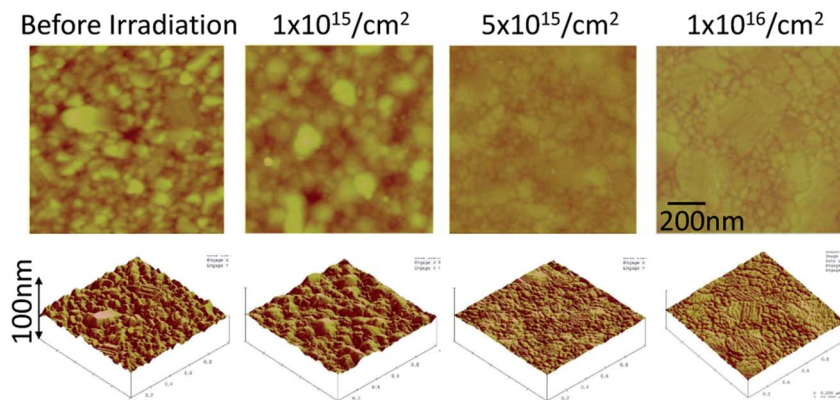


Fig. 1 AFM of 70 nm Ag before and after GCIB with 1×10^{15} to 1×10^{16} ions per cm^2 dose.

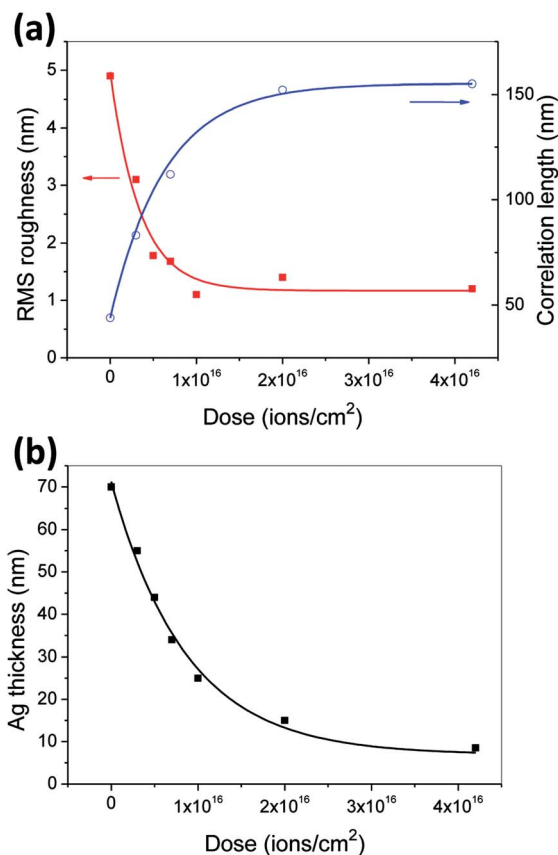


Fig. 2 (a) Plot of surface roughness, correlation length and (b) thickness as a function of dose. The line is an indication of the trend.

sputtering causes atoms to be deposited on the downward side of the hills. The red arrows show the migration of the Ag atoms towards the valley, voids or grain boundaries, resulting in a smoothing and flattening of the surface. As the irradiation increases, thickness of the film also reduces. The extra material deposited at the grain boundaries forms an amorphized Ag in this region. Eventually, this region is indistinguishable from the surrounding crystals, effectively increasing the lateral size of the grains. This is possible as the sputter depth is of similar dimension as R_{max} , peak-to-valley height.

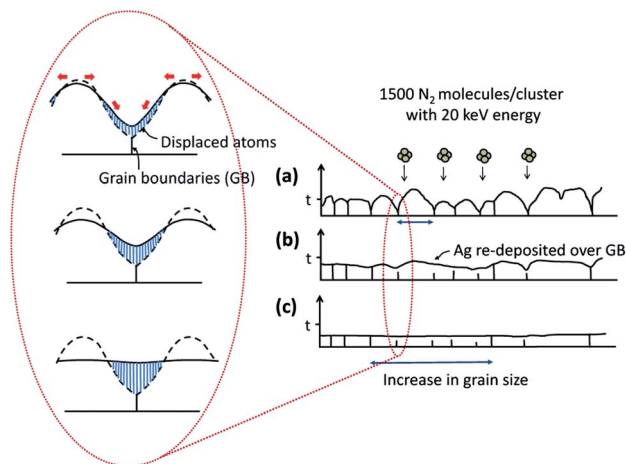


Fig. 3 (a–c) Schematic diagram showing the smoothing and thinning effect on polycrystalline Ag with increasing dose. A close-up view of the GCIB mechanism is illustrated too. The dotted lines represent the original surface before irradiation, and the red arrows represent the migration of the atoms. Thickness of the film is reduced from its initial thickness, t .

GCIB can be used as a novel method for making continuous ultrathin and smooth silver films by depositing a thicker starting layer and etching it to the desired thickness. Comparison of the SEM images in Fig. 4a and b shows an improved surface morphology and continuity with lower percolation threshold for ultrathin films formed by GCIB irradiation. Using a constant deposition rate of 1 A s^{-1} , the expected 10 nm film is discontinuous, being predominately made up of isolated crystallites and clusters. When the thickness increases to 13 nm, the film starts to form a connected network of elongated crystallites. This is the point when it changes from insulating to conducting. At 22 nm, the islands coalesce to form a continuous film, with small voids still visible in the layer. Also shown are ~ 3 nm, 5.8 nm and 15 nm Ag films formed after GCIB etching of 70 nm thick Ag layers with doses of 5.2×10^{16} , 5.0×10^{16} and 2×10^{16} ions per cm^2 (Fig. 4b). Even at a thickness of 15 nm, the film is continuous, consisting of large grains of 300 nm. Voids start to develop as the thickness reduces to 5.8 nm, but the film is still

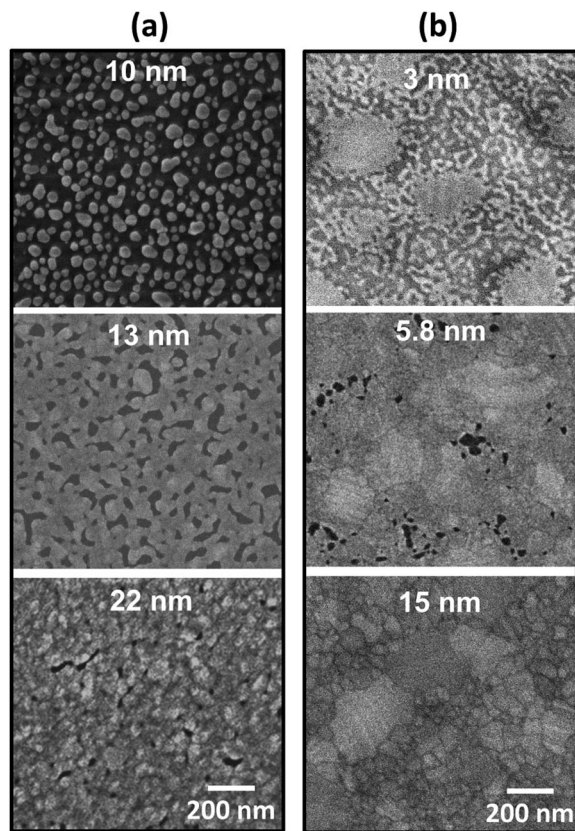


Fig. 4 SEM of (a) as-deposited 10 nm, 13 nm and 22 nm thick Ag as compared to (b) GCIB processed films of 3 nm, 5.8 nm and 15 nm thick Ag, produced by etching 70 nm thick with dose of 5.2×10^{16} , 5.0×10^{16} and 2×10^{16} ions per cm^2 respectively.

conducting. At ~ 3 nm, isolated islands of Ag of 300 nm can be seen. We estimate that the percolation threshold is about 4 nm for GCIB processed films, as compared to 11 nm for as-deposited films. The minimum thickness that can be obtained using this technique is not dependent on the substrate but rather on the uniformity of the beam irradiation.

Electrical and optical properties

We have investigated the electrical resistivity and optical properties of these films using Hall measurements and SPR spectroscopy. For comparison, we have also plotted the results obtained for Cr (2 nm)/Ag. In Fig. 5a, we can see that the electrical resistivity of as-deposited Ag films is similar to that of bulk silver at a thickness greater than 50 nm. Deviation from bulk resistivity starts to occur at a thickness below 30 nm and increases significantly to 4 times the bulk resistivity at 15 nm. Even though the Cr/Ag film is continuous and smoother ($\sigma = 2$ nm, $L = 20$ nm), it still shows higher resistivity compared to the as-deposited Ag film. The GCIB processed Ag films show a much lower resistivity compared to Ag and Cr/Ag films for thicknesses less than 30 nm. In fact, deviation from bulk values occurs at a much lower thickness of 12 nm.

SPR spectroscopy is used to determine the dielectric constant, ϵ_m , of these films, whereby the thickness is

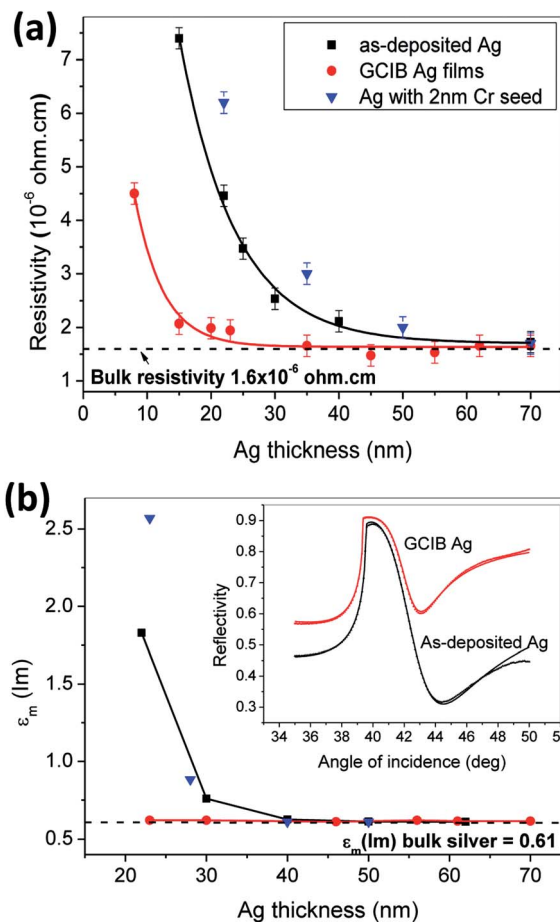


Fig. 5 (a) Electrical resistivity and (b) imaginary part of epsilon, ϵ_{Im} , for as-deposited Ag (square symbols), GCIB Ag (circle symbols) and Cr/Ag (triangle symbols) as a function of thickness. Inset shows the SPR curves for 22 nm thick as-deposited and GCIB films. The line is an indication of the trend.

predetermined using AFM. The bulk value $\epsilon = -16.0 + 0.6i$ (ref. 34) is obtained from Palik's data at 632.8 nm wavelength. Using sum of least square fit of the experimental to the calculated reflectivity, R_{cal} , in eqn (1), we are able to extract the dielectric constant of Ag.

$$R_{\text{cal}} = \left| \frac{r_{\text{gm}} + r_{\text{ma}} e^{2i\alpha_m d}}{1 + r_{\text{gm}} r_{\text{ma}} e^{2i\alpha_m d}} \right|^2 \quad (1)$$

where subscripts m, g and a denote metal, glass and air respectively, d is the thickness of the metal film. r_{ij} are the Fresnel reflection coefficients for p-polarization.

$$r_{ij} = \frac{\epsilon_j \alpha_i - \epsilon_i \alpha_j}{\epsilon_j \alpha_i + \epsilon_i \alpha_j} \quad \text{for } i, j = \text{g, m, a}$$

$$\alpha_j = \sqrt{\epsilon_j \left(\frac{\omega}{c}\right)^2 - k_{\parallel}^2} \quad \text{for } j = \text{g, m, a}$$

$$k_{\parallel} = \frac{\omega}{c} \sqrt{\epsilon_g} \sin \theta$$

where k_{\parallel} is the component parallel to the surface of the wave-vector of the incident light with angular velocity ω . c is the speed of light and θ is the angle of incidence. Inset of Fig. 5b shows the SPR curves of an as-deposited and a GCIB film for a thickness of 22 nm. It can be seen that the as-deposited film has a higher resonance angle and wider FWHM compared to the GCIB film. For the as-deposited Ag film, $\epsilon_m(\text{Im})$ starts to increase at the thickness of 30 nm, reaching a value that is 3 times higher at 22 nm (Fig. 5b). Similar behaviour in $\epsilon_m(\text{Im})$ is observed for the Cr/Ag film. On the other hand, no change is observed for $\epsilon_m(\text{Im})$ even at a thickness of 22 nm. From these studies, we show that GCIB is an effective method for improving the electrical and optical properties of ultrathin Ag and is especially useful for plasmonics application in the thickness regime of 10–30 nm.

In order to understand the effect of roughness on the damping loss, we have simulated the SPR curves with roughness and correlation length included *via* the metal permittivity at thicknesses of 55 nm and 22 nm (Fig. 6a–b).^{22,35} Roughness gives rise to a small change in SPP wave vector, Δk_{sp} from smooth metal surfaces. The effective permittivity with roughness, ϵ_{eff} , can be derived from $k_{\text{sp}}(\epsilon_{\text{eff}}) = k_{\text{sp}}(\epsilon_m) + \Delta k_{\text{sp}}$, where ϵ_m is the metal permittivity and Δk_{sp} can be calculated using a formula derived previously.³⁶ We can see that the resonance angle and FWHM increases for the rough as-deposited film

compared to the film with no roughness. This is consistent with our experimental data. Other groups have also reported a similar behavior of SPR curves when roughness are included.^{35,37} By reducing σ to 1.6 nm, it approaches that of the SPR curve with no roughness. Table 1 shows a comparison of the FWHM and surface plasmon propagation length, L_{SPP} , for the experimental and calculated SPR curves. The FWHM of the curve is extracted by fitting a Lorentzian equation to the curve. It can be seen that surface roughness of $\sigma = 5$ nm accounts for about 20–36% increase in FWHM and L_{SPP} , for both thicknesses. For a 55 nm thick as-deposited Ag film, the experimental FWHM matches the calculated results with roughness included. However, it is not enough to account for the 2 times wider FWHM obtained experimentally for a thickness of 22 nm. This means that scattering from defects and grain boundaries contributes more significantly to the increase in loss as the thickness drops below 30 nm. On the other hand, GCIB films with a surface roughness of $\sigma = 1.6$ nm show narrower FWHM and longer L_{SPP} , and roughness only accounts for less than 10% of the loss, matching closely to the simulation result. In fact, results are approaching that of the theoretical limit, indicating no additional contribution from grain boundaries or voids. Partial amorphization introduced by the irradiation process does not seem to increase the optical absorption of the material.

The sharp increase in resistivity and optical loss as thickness drops below 30 nm cannot be explained by surface roughness. For the as-deposited film, this could be due to the onset of voids developing in the film. Though depositing a Cr seed layer improves surface roughness and film continuity, it did not reduce the optical loss or resistivity. From these, we can isolate that the main contributing factor for the increase in loss is due to grain boundaries scattering from smaller crystallites. For GCIB processed films, we observe a 3 times increase in correlation length from 44 nm to 152 nm, indicative of the corresponding increase in grain width. From the SEM images, the film is still continuous at a thickness of 15 nm. The larger grain width and improved film continuity results in much better electrical and optical properties in ultrathin regime. An ultrathin 12 nm film can have the same plasmonic behavior as bulk Ag. This is especially important for improving the contrast and resolution of Ag superlens, and multilayer composite hyperlens, which is one of the main obstacles facing this technology.

Nano-processing on lithographically patterned waveguide

In this last section, we show that GCIB can be applied to a lithographically patterned Ag stripe waveguides. SNOM was performed on 5 μm wide waveguides before and after GCIB, using a wavelength of 632.8 nm (Fig. 7a). Light is coupled into the metallic waveguide using gratings seen in Fig. 7b. By fitting the intensity profile along the waveguide with an exponential decay, we are able to extract its propagation length. Before GCIB, the waveguide is 50 nm thick and has a propagation length of about 3.10 μm . After GCIB processing, the Ag thickness is reduced to 30 nm and the propagation length is increased to 3.58 μm . We have compared our results with simulations using the finite element method (FEM), with Palik's

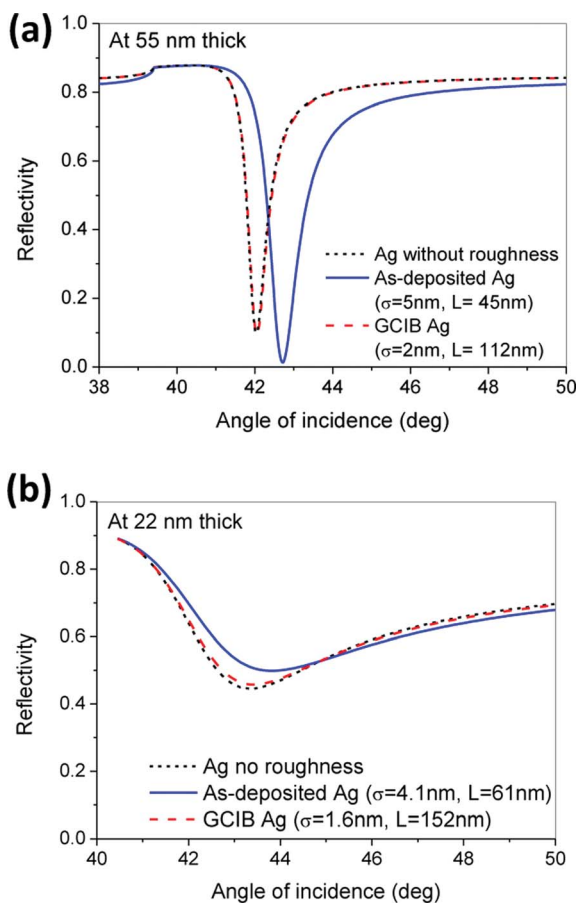


Fig. 6 Calculated SPR curves with and without roughness for (a) 55 nm and (b) 22 nm thick Ag.

Table 1 Experimental and calculated FWHM with surface roughness, σ , and correlation length, L incorporated for thicknesses of 22 nm and 55 nm. Also plotted is the calculated L_{SPP}

Samples	Thickness (nm)	σ (nm)	L (nm)	Experimental FWHM ($^\circ$)	Calculated FWHM ($^\circ$)	Calculated L_{SPP} (μm)
Ag (no roughness)	22	0	0	—	2.60	1.54
GCIB Ag		1.6	152	2.55	2.63	1.53
As-deposited Ag		4.1	61	5.70	3.38	0.98
Ag (no roughness)	55	0	0	—	0.49	4.62
GCIB Ag		2.0	112	0.55	0.53	4.61
As-deposited Ag		5.0	45	0.62	0.60	3.36

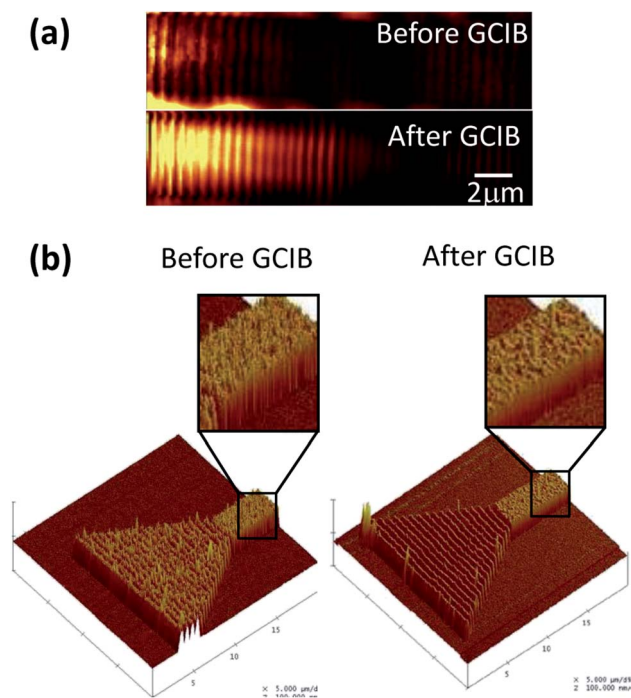


Fig. 7 (a) SNOM images and (b) AFM images of Ag stripe waveguide. A close-up of the smoother sidewalls seen after GCIB irradiation.

data.³⁴ The FEM simulated L_{SPP} of a $5 \mu\text{m} \times 50 \text{nm}$ waveguide is $7 \mu\text{m}$, while that of $5 \mu\text{m} \times 30 \text{nm}$ waveguide is approximately $4 \mu\text{m}$. The $\sim 55\%$ discrepancy between the experimental and simulated results of the as-deposited Ag films could be due to the higher surface roughness. The propagation length of the GCIB processed waveguide is in agreement with simulation result. This confirms the fact that there is no additional loss due to roughness and defects, and negligible damage is incurred from the GCIB process. From the AFM images of the waveguides (Fig. 7b), a significant improvement in roughness is observed not only from the top surfaces, but also from the sidewalls of the waveguides. This demonstrates the effectiveness of GCIB for conformal smoothing of metallic nanostructures, without modifying the edge profile. As there is no seed layer used, the Ag layers tend to peel off with prolong laser irradiation. This may result in poorer coupling efficiency into the as-deposited waveguide. However, GCIB irradiated waveguides appear intact after characterization, indicating that there is a stronger

adhesion to the substrate. This is another important aspect to consider if Ag plasmonic nanostructures are to be used.

Conclusions

We have shown direct evidence that surface roughness is not the main loss mechanism in plasmonic structures and scattering from grain boundaries and voids contribute more significantly to the increase in loss in ultrathin regime. Using the unique characteristics of cluster beam irradiation, we are able to achieve shallow surface smoothing down to 1.2 nm and precise etching in Ag films and lithographically patterned structures with nanometer resolution. This is accompanied by a 3 times increase in grain width, as a result of re-deposition of Ag atoms in the grain boundaries. The improved film continuity is also demonstrated by the reduced percolation threshold from 11 nm to 4 nm. Significant improvement in electrical and optical properties of up to 4 times can be obtained in these films, before deviation from bulk silver properties starts to occur at 12 nm. By applying it post fabrication to lithographically patterned waveguide, we show conformal smoothing of surfaces with enhanced surface plasmon propagation. This provides a nano-scale processing tool for fabrication of ultrathin plasmonics and metamaterials devices with low loss.

Acknowledgements

This work was supported by A*STAR under Grant no. 0921540098 and 0921540099, and plasmonics optical fiber sensor grant (IMRE/12-1C0301).

References

- 1 Y. Xiong, Z. Liu, C. Sun and X. Zhang, *Nano Lett.*, 2007, 7, 3360.
- 2 Z. W. Liu, H. Lee, Y. Xiong, C. Sun and X. Zhang, *Science*, 2007, 315, 1686.
- 3 A. V. Kildishev and V. M. Shalaev, *Opt. Lett.*, 2008, 33, 43.
- 4 J. B. Pendry, *Phys. Rev. Lett.*, 2000, 85, 3966.
- 5 N. Fang, H. S. Lee, C. Sun and X. Zhang, *Science*, 2005, 308, 534.
- 6 T. Xu, A. Agrawal, M. Abashin, K. J. Chau and H. J. Lezec, *Nature*, 2013, 497, 470.
- 7 I. D. Leon and P. Bernini, *Nat. Photonics*, 2010, 4, 382.

- 8 P. B. Johnson and R. W. Christy, *Phys. Rev. B: Solid State*, 1972, **6**, 4370.
- 9 H. W. Edwards and R. P. Petersen, *Phys. Rev.*, 1936, **50**, 871.
- 10 S. A. Ramakrishna, J. B. Pendry, M. C. K. Wiltshire and W. J. Stewart, *J. Mod. Opt.*, 2003, **50**, 1419.
- 11 H. Liu, B. Wang, L. Ke, J. Deng, C. C. Choy, M. S. Zhang, L. Shen, S. A. Maier and J. H. Teng, *Adv. Funct. Mater.*, 2012, **22**, 3777.
- 12 H. K. Yuan, U. K. Chettiar, W. S. Cai, A. V. Kildishev, A. Botasseva, V. P. Drachev and V. M. A. Shalaev, *Opt. Express*, 2007, **15**, 1076.
- 13 Y. Chi, E. Lay, T. Y. Chou, Y. H. Song and A. Carty, *Chem. Vap. Deposition*, 2005, **11**, 206–212.
- 14 F. Jing, H. Tong, L. Kong and C. Wang, *Appl. Phys. A: Mater. Sci. Process.*, 2005, **80**, 597.
- 15 L. L. Yin, V. K. V. Vlasko, J. Pearson, J. M. Hiller, J. Hua, U. Welp, D. E. Brown and C. W. Kimball, *Nano Lett.*, 2005, **5**, 1399.
- 16 S. Kundu, S. Hazra, S. Banerjee, M. K. Sanyal, S. K. Mandal, S. Chaudhuri and A. K. Pal, *J. Phys. D: Appl. Phys.*, 1998, **31**, L73.
- 17 X. Sun, R. Hong, H. Hou, Z. Fan and J. Shao, *Chin. Opt. Lett.*, 2006, **4**, 366.
- 18 W. Chen, M. D. Thoreson, S. Ishii, A. V. Kildishev and V. M. Shalaev, *Opt. Express*, 2010, **18**, 5124.
- 19 V. Logeeswaran, N. P. Kobayashi, M. S. Islam, W. Wu, P. Chaturvedi, N. X. Fang, S. Y. Wang and R. S. Williams, *Nano Lett.*, 2009, **9**, 178.
- 20 W. Chen, K. P. Chen, M. D. Thoreson, A. V. Kildishev and V. M. Shalaev, *Appl. Phys. Lett.*, 2010, **97**, 211107.
- 21 A. Pinchuk, U. Kreibig and A. Hilger, *Surf. Sci.*, 2004, **557**, 269.
- 22 H. Liu, B. Wang, E. S. P. Leong, P. Yang, Y. Zong, G. Si, J. Teng and S. A. Maier, *ACS Nano*, 2010, **4**, 3139.
- 23 H. Liu, B. Wang, L. Ke, J. Deng, C. C. Chum, S. L. Teo, L. Shen, S. A. Maier and J. H. Teng, *Nano Lett.*, 2012, **12**, 1549.
- 24 P. Nagpal, N. C. Lindquist, S. H. Oh and D. J. Norris, *Science*, 2009, **325**, 594.
- 25 N. Toyoda, Nano-processing using Gas Cluster Ion Beam, Ph.D thesis, Kyoto University, March 1999.
- 26 I. Yamada and N. Toyoda, *Nucl. Instrum. Methods Phys. Res., Sect. B*, 2005, **241**, 589.
- 27 E. Bourelle, A. Suzuki, A. Sato, T. Seki and J. Matsuo, *Nucl. Instrum. Methods Phys. Res., Sect. B*, 2005, **241**, 622.
- 28 A. Kirkpatrick, *Nucl. Instrum. Methods Phys. Res., Sect. B*, 2003, **206**, 830.
- 29 I. Yamada and J. Khoury, *MRS Online Proc. Libr.*, 2011, **1354**.
- 30 M. Yano, M. Fukui, M. Haraguchi and Y. Shintani, *Surf. Sci.*, 1990, **227**, 129.
- 31 W.-J. Lee, J.-E. Kim, H. Y. Park, S. Park, M.-S. Kim, J. T. Kim and J. J. Ju, *J. Appl. Phys.*, 2008, **103**, 073713.
- 32 W. Knoll, *Annu. Rev. Phys. Chem.*, 1998, **49**, 569.
- 33 M. Hinojosa, E. Bouchaud and B. Nghiem, *MRS Online Proc. Libr.*, 2011, **539**.
- 34 E. D. Palik, *Handbook of Optical Constants of Solids*, Academic Press, New York, 1991.
- 35 A. Kolomenski, A. Kolomenskii, J. Noel, S. Y. Peng and H. Schuessler, *Appl. Opt.*, 2009, **48**, 5683.
- 36 E. Fontana and R. H. Pantell, *Phys. Rev. B*, 1988, **37**, 3164.
- 37 A. Hoffmann, Z. Lenkefi and Z. Szentirmay, *J. Phys.: Condens. Matter*, 1998, **10**, 5503.